Published in final edited form as:
Biomaterials. 2015 February ; 0: 141–150. doi:10.1016/j.biomaterials.2014.11.012.

Pharmacodynamics of long-acting folic acid-receptor targeted ritonavir boosted atazanavir nanoformulations

Pavan Puligujja[1], **Shantanu Balkundi**[1], **Lindsey Kendrick**[1], **Hannah Baldridge**[1], **James Hilaire**[1], **Aditya N. Bade**[1], **Prasanta K. Dash**[1], **Gang Zhang**[1], **Larisa Poluektova**[1], **Santhi Gorantla**[1], **Xin-Ming Liu**[1,3], **Tianlei Ying**[4,5], **Yang Feng**[4], **Yanping Wang**[4], **Dimiter S. Dimitrov**[4], **JoEllyn M. McMillan**[1], and **Howard E. Gendelman**[1,3,*]

[1]Department of Pharmacology and Experimental Neuroscience, University of Nebraska Medical Center, Omaha, NE, 68198-5880 USA

[2]Kansas University Innovation and Collaboration, Lawrence, KS, 66045, USA

[3]Department of Pharmaceutical Sciences, University of Nebraska Medical Center, Omaha, NE, 68198-5880 USA

[4]Protein Interactions Group, Laboratory of Experimental Immunology, Cancer and Inflammation Program, Center for Cancer Research, National Cancer Institute, National Institutes of Health, Frederick, Maryland 21702, USA

[5]Key Laboratory of Medical Molecular Virology of Ministries of Education and Health, Shanghai Medical College and Institute of Medical Microbiology, Fudan University, Shanghai 200032, China

Abstract

Long-acting nanoformulated antiretroviral therapy (nanoART) that target monocyte-macrophage could improve the drug's half-life and protein binding capacities while facilitating cell and tissue depots. To this end, ART nanoparticles that target the folic acid (FA) receptor and permit cell-based drug depots were examined using pharmacokinetic and pharmacodynamic (PD) tests. FA receptor-targeted poloxamer 407 nanocrystals, containing ritonavir-boosted atazanavir (ATV/r), significantly affected several therapeutic factors: drug bioavailability increased as much as 5 times and PD activity improved as much as 100 times. Drug particles administered to human peripheral blood lymphocyte reconstituted NOD.Cg-*Prkdc*^{scid}*Il2rg*^{tm1Wjl}/SzJ mice and infected with HIV-1_{ADA} at a tissue culture infective dose50 of 10^4 infectious viral particles/ml led to ATV/r drug concentrations that paralleled FA receptor beta staining in both the macrophage-rich parafollicular areas of spleen and lymph nodes. Drug levels were higher in these tissues than what could be achieved by either native drug or untargeted nanoART particles. The data also mirrored potent reductions in viral loads, tissue viral RNA and numbers of HIV-1p24+ cells in infected and

*Address correspondence to: Howard E. Gendelman, Department of Pharmacology and Experimental Neuroscience, 985880 Nebraska Medical Center, Omaha, NE, USA 68198-5880, Phone: (402) 559-8920, Fax: (402) 559-3744, hegendel@unmc.edu.

treated animals. We conclude that FA-P407 coating of ART nanoparticles readily facilitate drug carriage and facilitate antiretroviral responses.

Keywords

folic acid receptor; long-acting nanoformulated antiretroviral therapy; human immunodeficiency virus type one; pharmacokinetics; pharmacodynamics; non-obese diabetic severe combined immunodeficient mice

Introduction

The development of long-acting nanoformulated antiretroviral therapy (nanoART) has now been realized, reflecting its evolution from theory to laboratory cell culture testing to animal studies to human clinical trials [1, 2]. However, the transition from academic research setting to clinical patient care has yet to be realized. The needs, nonetheless, to make nanoART accessible are immediate as limitations in ART adherence, drug fatigue, emergence of viral resistance, and restrictions of drug penetration to viral reservoirs abound [3–5]. Daily or twice daily drug administrations have a myriad of restrictions in resource-limited settings, during co-morbid conditions such as malabsorption syndromes and by concomitant substance abuse. These underlie the long-term success of currently available therapies [6–9] and are accentuated by the lifelong ART needs.

There are several properties related to the drug and its formulation that pose obstacles towards the broad use of nanoART. These include the chemical and pharmacologic properties of ART, such as its half-life, protein binding and hydrophobicity capacities. Additional limitations for long-term administration revolve around adverse drug events limited by an inability to rapidly remove ART from circulation. These have proved to be substantive hurdles for medicinal chemists seeking to translate oral daily dosing into a once a week, once a month or every 2–6 months injectable formulation [10, 11]. Nonetheless, advantages for longer term ART abound. These include maintenance of steady state drug levels to limit the development of viral resistance to any antiretroviral, thus offsetting the consequences of poor ART compliance to daily dosing [12]. Yet, additional limitations of ART include adherence to drug regimens and the continuous long-term access to the medicines that are required during lifelong therapy. For these reasons, amongst others, long-term ART has ascended to the center stage of international research activities [2, 11].

Others and our laboratory have taken the concept of longer acting ART to yet another potential level [12, 13]. That level is now referred to as cell- and tissue-targeted nanoART [13]. Here, the overarching idea is to synthesize nanoART with targeted ligands that facilitate its entry into viral target cells and tissues. This would prolong the intracellular drug depots and further extend the drug's half-life [13]. The idea also stems from evidence that sustained quantities of virus persist in lymphoid tissues such as the spleen, lymph nodes, gut-associated lymphoid tissue (GALT) and brain [14, 15]. Hence, long-acting nanoART with infrequent administration could lead to drug retention in subcellular compartments and to stable therapeutic ART concentrations in viral sanctuaries [13, 16, 17]. The advantages of biocompatible polymers, such as poloxamer 407 (P407) and poloxamer 188 (P188)

covalently linked to folic acid (FA) for encapsulating known hydrophobic antiretroviral drugs such as atazanavir (ATV) and ritonavir (RTV) have been reported [18, 19]. These nanoparticle-based RTV boosted ATV (nanoATV/r or P407-ATV/r) formulations show increased retention and slow drug dissociation inside a human monocyte-derived macrophage (MDM) carrier [16]. Improvements in intracellular drug targeting were achieved by coating nanoART with FA-P407 [13]. We now demonstrate that FA particle coating substantially improves drug pharmacokinetics (PK) and pharmacodynamics (PD) with enhanced distribution of drug to the reticuloendothelial system such as lymphoid tissues and liver. Receptor expression is enhanced on tissue macrophages as a consequence of nanoART administration providing autocrine enhancement for drug distribution. Moreover, when FA-nanoATV/r is parentally administered through an intramuscular route, plasma drug levels are increased up to 5-fold; and the concentration of drug required to achieve a 50% effective inhibitory concentration (IC_{50}) for mice was reduced from 250 to 50 mg/Kg [13]. Pre-exposure prophylaxis (PrEP) measured antiretroviral responses of the FA-nanoATV/r in human peripheral blood lymphocytes (Hu-PBL) reconstituted-NOD/*scid*, IL2 receptor gamma chain knockout, NOD.Cg-*Prkdc*^{scid}*Il2rg*^{tm1Wjl}/SzJ (NSG) mice that were infected with HIV-1_{ADA}. The mice showed rapid viral reductions by measures of number of HIV-1p24+ cells in lymphoid tissue and polymerase chain reaction (PCR) for viral RNA. The pharmacodynamics seen by PrEP were validated in a chronic infection model of HIV/AIDS where HIV-1_{ADA} infected $CD34^+$ human stem cell (HSC) transplanted NSG mice were treated every other week with parenteral intramuscular injections FA-nanoATV/r. The results showed viral RNA copies at or below the levels of detection. These results, taken together, demonstrate the role for FA nanoART targeting in improving drug PK and PD. As such this strategy would enable decreased drug dosing for long-acting nanoART nanoformulations. The development of such a targeting scheme for human use is now being forged.

Materials and Methods

Chemicals

ATV-sulfate was purchased from Gyma Laboratories of America Inc. (Westbury, NY, USA) and free-based using triethylamine. Free-base RTV was purchased from Shengda Pharmaceutical Co (Zhejiang, China). P407 and FA were purchased from Sigma-Aldrich (St. Louis, MO, USA). Pooled human serum was purchased from Innovative Biologics (Herndon, VA, USA). For macrophage colony-stimulating factor (MCSF) preparation, 5/9 alpha3–18 cells (ATCC) were cultured in ATCC complete growth medium and recovered supernatant fluids used as a media supplement at 10% volume [20].

Manufacture and characterization of FA-P407-ATV/r

FA-P407 was synthesized and used to manufacture FA-nanoATV/r [13]. Briefly, FA-P407 (0.2% w/v) and P407 (0.3% w/v) were mixed in 10mM HEPES to generate micelles; 1% (w/v) drug was added and mixed overnight. For preparation of FA-P407-ATV and FA-P407-RTV, 0.5% (w/v) P407 was mixed with 1% drug. The nanosuspensions were homogenized at 20,000 PSI using an Avestin Emulsiflex C3 homogenizer (Avestin Inc, Ottawa, ON, Canada) until the desired particle size (300–400 nm) was reached. Free

polymers and non-encapsulated drug particles were removed by centrifugation; the nanoparticles were resuspended in 0.2% P407. The resulting nanosuspension was lyophilized and stored in a desiccator protected from light. Drug loading was determined using reversed phase high-performance liquid chromatography (HPLC) and ultra-performance liquid chromatography tandem mass spectrometry (UPLC-MS/MS) as described [13]. Particle size, polydispersity and zeta potential for the nanoformulations were determined by dynamic light scattering using a Malvern Zetasizer Nano-ZS instrument (Malvern Instruments Inc., Westborough, MA, USA).

Mouse FA receptor beta (mFRβ) Fabs and conversion to IgG2a

A large phage display library was constructed by using peripheral blood mononuclear cells (PBMC) cDNA from 40 healthy volunteers as templates for cloning the expressed antibody gene repertoire. The library was panned using recombinant ectodomain of mFRβ conjugated to magnetic beads (Invitrogen, Carlsbad, CA, USA). Amplified libraries of 10^{12} phage-displayed Fabs were incubated with 5, 3, 2 and 1 μg of mFRβ for 2 h at room temperature during the first, second, third and fourth rounds of biopanning, respectively. Clones that bound to mFRβ were identified from the third and fourth rounds of panning by using monoclonal phage ELISA. The VH and VL domains of these clones were sequenced and used to generate a full-size antibody in a mouse IgG2a format. The IgG2a was expressed in mammalian cells and purified. Protein purity was estimated as >95% by SDS-PAGE, and protein concentration was measured spectrophotometrically (NanoVue, GE Healthcare, Piscataway, NY).

Isolation and transplantation of human cells

Human peripheral blood lymphocytes (hu-PBL) and monocytes were isolated by leukapheresis from HIV-1 and hepatitis seronegative individuals by counter-current centrifugal elutriation [21]. For reconstitution 25×10^6 hu-PBL per mouse were injected intraperitoneally into 8–10 week old NOD/SCID/IL2Rγc$^{-/-}$ (NSG) mice obtained from a University of Nebraska Medical Center (UNMC) breeding colony under an approved UNMC Institutional Animal Care and Use protocol as previously described [22].

Immunohistochemical staining

Male Balb/cJ mice 6–8 weeks of age (Jackson Labs, Bar Harbor, ME) were injected intramuscularly (IM) with PBS or FA-P407-ATV/RTV (FA-nanoATV/r; 100 mg/kg each drug) and sacrificed 36 hours post treatment. Spleens were collected and fixed with 10% neutral buffered formalin. The protocols used by Vector® Mouse on Mouse (M.O.M.™) ImmPRESS HRP (peroxidase) Polymer kit (Vector Laboratories, Burlingame, CA, USA) were followed for decreasing the background on mouse sections. The spleen sections were stained with a 1:200 dilution of the mFRβ-specific antibody, washed and stained with M.O.M anti-mouse secondary antibody (Vector laboratories), followed by 3,3-diaminobenzidine (DAB) staining. Cell nuclei were stained with Mayer's hematoxylin.

For HIV-1p24 staining, virus-infected hu-PBL-NSG mouse tissues were collected at day 14 in 10% neutral buffered formalin and embedded in paraffin. Successive 5 μm thick tissue sections were stained with mouse monoclonal antibodies for HIV-1p24 (clone Kal-1; 1:10)

and human leukocyte antigen HLA-DR (clone CR3/43; 1:100), respectively. The secondary antibodies were polymer-based DAKO envision systems linked to horseradish peroxidase. The sections were developed with DAB. The nuclei were counterstained with Mayer's hematoxylin. The slides were visualized with a 40X objective on a Nikon Eclipse E800 microscope using NIS-Elements F 3.0 software (Nikon Instruments). The number of HIV-1p24+ cells and number of HLA-DR+ cells per section were counted and expressed as percentage of HIV-1p24+ cells/HLA-DR+ cells in a section.

FA-nanoATV/r PK and PD

Male Balb/cJ mice (Jackson Labs), 8 weeks old, were maintained on folate-deficient diet (Harlan Teklad TD.00434, Harlan Laboratories, Indianapolis, IN) for 2 weeks then injected with either 50 or 100 mg/kg of P407-ATV/r or FA-P407-ATV/r. Plasma was collected 7 or 14 days later for drug analysis. The mice were sacrificed on day 14; tissues were collected and stored at −80°C. Plasma and tissue drug levels were determined using UPLC-MS/MS as previously described [23]. For PD studies NSG mice (8–10 weeks old) were maintained on a folate deficient diet for 1 week prior to hu-PBL reconstitution and throughout the study. One week following reconstitution, mice were treated with 10, 50 or 100 mg/kg of P407-ATV/r or FA-P407-ATV/r. Native drug controls were treated with 10 or 50 mg/kg non-formulated ATV/r. The mice were infected one day after drug treatment by intraperitoneal injection with HIV-1_{ADA} at a tissue culture infective $dose_{50}$ ($TCID_{50}$) of 10^4 per mouse. Blood samples were collected from facial vein one day before and 2 or 3, 7 and 14 days after treatment (Figure 1A). All animal protocols were performed in accordance with the UNMC Institutional Animal Care and Use Committee requirements. The scheme for infection and treatment are presented in Figure 1A. Alternately, a chronic infection model was used where five month NSG mice were transplanted with $CD34^+$ hematopoietic stem cells (HSC). The animals were infected with HIV-1_{ADA} intraperitoneally for five weeks at 10^4 tissue culture infective dose50, $TCID_{50}$/mouse. Infected mice were either treated with 100 mg/kg FA-ATV/r or untreated. A boosting dose was administered at two and four weeks after the first dose. The mice were sacrificed at week 6 and plasma was collected to determine viral loads. The mice were maintained on folate deficient diets for the duration of the experiment.

Flow cytometry

Blood samples were collected into Ca^{2+}-ethylenediaminetetraacetic acid (EDTA)-coated tubes before infection and 1 and 2 weeks following treatment. Spleen cells were isolated after sacrifice on day 14. The blood and spleen cells were analyzed by flow cytometry for the presence of human pan-CD45, CD3, CD4 and CD8 immune markers as previously described [24].

HIV-1 RNA PCR and viral load determinations

Spleens were isolated at the time of animal sacrifice and RNA was extracted using TRIzol (Invitrogen). Moloney murine leukemia virus reverse transcriptase (Invitrogen) and random hexamers were used for reverse transcribing RNA to cDNA [25]. Quantitative RT-PCR was performed to estimate the HIV-1*gag* RNA levels. Similarly, RT-PCR was performed to determine human CD45 and GAPDH RNA levels. Plasma from CD34+ HSC transplanted

NSG mice were analyzed for viral RNA copies/ml before and after treatment using COBAS Amplicor System v1.5 (Roche Molecular Diagnostics, Switzerland) [26].

Statistical analyses

The data are presented as mean ± SEM. Statistical significance between groups was assessed using Mann-Whitney U-test by Graph-Pad® Prism unless specified. The data were considered statistically significant if $P < 0.05$.

Results

Physicochemical characterization of nanoformulations

NanoATV/r were manufactured by high-pressure homogenization as previously described. Particle size, charge and polydispersity index for all formulations were determined by dynamic light scattering [18, 27, 28]. Both ATV and RTV nanoparticles were rod-shaped and negatively charged with zeta potential from −6 to −25 mV. The particles were uniformly distributed with polydispersity indices (PDI) between 0.10 and 0.25. FA-nanoATV had a particle size of 374 ± 3 nm with PDI of 0.23 ± 0.01 and zeta potential of −14.0 ± 0.6 mV. FA-nanoRTV had a particle size of 390.1 ± 22 nm, with PDI of 0.21 ± 0.01 and zeta potential of −6 ± 10 mV. The non-targeted nanoATV/r showed similar physicochemical measurements. Drug loading of the nanoformulations was determined by HPLC as previously described [13]. Drug loadings for FA-nanoATV and FA-nanoRTV nanoformulations were from 45 to 75% depending upon the purification efficiency.

Mouse folate receptor distribution

Balb/cJ mice were administered IM either PBS or 100 mg/kg P407-ATV/r. The mice were then sacrificed 36 hours post treatment. The spleens were fixed and stained with a mFRβ-specific antibody followed by anti-mouse secondary antibody and hematoxylin staining. Representative images of these stained sections are shown in Figure 1B and 1C. NanoART treatment itself appeared to increase the level of folate receptor expression in spleen compared to PBS treatment.

PK of FA-nanoATV/r

PK and biodistribution of non-targeted and targeted nanoART were studied in Balb/cJ mice. The mice were injected with either 50 or 100 mg/kg of FA-P407-ATV/r or P407-ATV/r and sacrificed on day 14. The plasma ATV concentrations following treatment with FA-P407-ATV/r were significantly higher than with P407-ATV/r and were dose dependent. The mean plasma ATV concentrations at day 14 with a 100 mg/kg dose were 344 ng/ml and 31 ng/ml for FA-P407-ATV/r and P407-ATV/r, respectively. Additionally, a 50 mg/kg dose of FA-nanoATV/r gave a plasma concentration of 154 ng/ml compared to 20 ng/ml ATV following non-targeted nanoATV/r (Figure 2A). Both doses provided ATV plasma concentrations above the minimum effective concentration (MEC) of 150 ng/ml [29]. The RTV plasma concentrations were not different between FA-nanoATV/r and nanoATV/r treatment groups. Tissue drug concentrations showed similar trends and were also dose dependent. A 100 mg/kg FA-P407-ATV/r dose gave 5270 ng/g and 204 ng/g ATV concentrations in liver and spleen compared to 142 ng/g and 57 ng/g in liver and spleen following P407-ATV/r

treatment. Alternately, the RTV tissue concentrations following FA-P407-ATV/r were 338 ng/g and 49 ng/g compared to 89 ng/g and 38 ng/g for P407-ATV/r in liver and spleen, respectively (Figure 2B). Similar observations were found in tissue drug concentrations for P407-ATV/r and FA-P407-ATV/r. Furthermore, Balb/cJ mice injected with 50 mg/kg FA-nanoATV/r and nanoATV/r showed comparable trends for ATV and RTV concentrations. PK was also measured in hu-PBL reconstituted NSG mice treated with 10, 50 or 100 mg/kg targeted and non-targeted nanoATV/r. The plasma and tissue concentrations were again dose-dependent. The mean plasma ATV concentrations at day 14 with a 10 mg/kg dose were 11 ng/ml and 18 ng/ml for nanoATV/r and FA-nanoATV/r, respectively, which was below the MEC. However, following a 50 mg/kg dose, the average ATV plasma concentrations for nanoATV/r and FA-nanoATV/r were 49 and 92 ng/ml, respectively. At a dose of 100 mg/kg nanoATV/r and FA-nanoATV/r, the observed plasma levels were 78 ng/ml and 183 ng/ml for ATV at day 14, respectively (Figure S1). These results correlated with our observations in Balb/cJ mice. The average ATV concentrations at day 14 with 50 mg/kg of FA-nanoATV/r were 326.8 ng/g in liver, 54.4 ng/g in spleen, 68.8 ng/g in lung compared to 102.1 ng/g in liver, 101.8 ng/g in spleen, and 50.4 ng/g in lung for nanoATV/r. In contrast, ATV concentrations at day 14 with 100 mg/kg of FA-nanoATV/r were 506 ng/g for ATV in liver, 131 ng/g in spleen, 199 ng/g in kidney and 83.04 in lung compared to 437 ng/g in liver, 144 ng/g in spleen, 87 ng/g in kidney and 58.4 ng/g in lung for nanoATV/r (Figure S2). The variability in drug concentrations for these tissues was attributed to the inherent variations in PBL reconstitution of the mouse model. The associations between drug levels, antiretroviral efficacy and immune modulatory activities were studied by determining HIV-1p24 antigen and *gag* RNA levels, and quantitation of CD4+ T cell numbers.

CD45+, CD3+, CD4+ and CD8+ T cells

For these studies, blood was collected from hu-PBL-NSG mice 2 days before and 1, 6 and 13 days after viral infection. Human CD4+ and CD8+ T cell counts were determined among CD3+ T cell populations. Levels of CD45+ T cells were evaluated to assess reconstitution of human cells amongst groups. The percentages of CD45+ T cells ranged from 21 to 49, 14 to 71 and 17 to 61% for 10 mg/kg, 50 mg/kg and 100 mg/kg, respectively (unpublished data). Mice were distributed into groups normalized for CD45+ T cell reconstitution. CD4+ T cell populations and CD4:CD8 ratios were decreased after 14 days relative to start times both in spleen and blood. The mice treated with nanoATV/r and FA-nanoATV/r showed preservation of both CD4+ T cells and CD4:CD8 ratios. At a dose of 100 mg/kg the mean ± SEM CD4:CD8 ratio for uninfected controls at day 14 in blood was 0.30 ± 0.01. FA-P407-ATV/r and P407-ATV/r treatment completely restored these ratios with a mean of 0.38 ± 0.20 and 0.51 ± 0.07 respectively (Figure 3A). For a 50 mg/kg dose, the mean ± SEM CD4:CD8 ratios for FA-P407-ATV/r and P407-ATV/r were 1.54 ± 0.77 and 1.76 ± 0.61 (Figure 3B) respectively compared to 9.80 ± 5.07 for uninfected mice. Both the groups restored CD4:CD8 ratios up to ~17% compared to 3% for the PBS treated group. The CD4+ T cell percentages for 50 mg/kg FA-nanoATV/r were from 31 to 84% in blood and 27 to 52% in spleen. For 100 mg/kg of FA-nanoATV/r, the CD4:CD8 T cell ratios in spleen were 0.1 to 0.6 compared to 0.03 to 0.1 for PBS controls, and the means were significantly different ($P<0.05$) (Figure 3A, 3B and 3C). However, there were no significant differences between nanoATV/r and FA-nanoATV/r or FA-nanoATV/r and saline in blood at all doses

(Figure 3A, 3B and 3C). One possible explanation is the limitations in immune restoration observed within the hu-PBL-NSG HIV model. These limitations would be overcome in a chronic model of HIV infection as previously reported in CD34+ humanized mice [30].

Antiretroviral activities

We evaluated levels of HIV-1p24 antigen in paraffin-embedded sections of liver, spleen (Figure 4), lung and kidney. A dose of 10 mg/kg with all treatments did not elicit protection from viral infection. In contrast, mice treated with 50 and 100 mg/kg of nanoATV/r and FA-nanoATV/r showed diminished HIV-1p24 antigen expression (Figure 5A and 5B). In the FA-nanoATV/r (50 mg/kg) group, 4/5 mice showed ≤ 2% of viral p24 expression compared to 1/7 in the nanoATV/r group in spleen. In the liver, the percent of HIV-1p24 for FA-nanoATV/r (50 mg/kg) varied from 0 to 24 compared to 0 to 43 for nanoATV/r. The differences between the groups were statistically significant ($P < 0.05$) (Figure 5B). Furthermore, all 6 mice had ≤ 2% of HIV-1p24 expression in spleen, liver and lung for FA-nanoATV/r (100 mg/kg) group. The P407-nanoATV/r group had 4/7 mice ≤ 2% in spleen, liver and lung. Also, the average HIV-1p24 expression was statistically different between FA-nanoATV/r and nanoATV/r groups in liver and lung at 100 mg/kg ($P < 0.05$) (Figure 5A). The decrease in HIV-1p24 antigen was dose dependent for both nanoATV/r and FA-nanoATV/r in liver, spleen and lung.

Next, we measured HIV-1*gag* RNA levels in the 50 and 100 mg/kg treatment groups by reverse transcriptase polymerase chain reaction (RT-PCR) assay. For the 100 mg/kg dose, the mean levels of HIV-1*gag* RNA normalized to human CD45 RNA levels were 5.8×10^3, 2.83×10^2 and 1.5×10^1 for PBS, nanoATV/r and FA-nanoATV/r treated, respectively (Figure 6A). The FA-P407-ATV/r and P407-ATV/r treatments both significantly reduced HIV-1*gag* RNA levels compared to the PBS treated group ($P < 0.05$). Alternatively, the mean HIV-1*gag* RNA normalized to CD45 RNA levels was 7×10^0 for FA-nanoATV/r and 6.8×10^2 for nanoATV/r for the 50 mg/kg dose (Figure 6B). Overall, the FA-nanoATV/r group showed statistically significant reduction in HIV-1*gag* RNA levels compared to the nanoATV/r and untreated groups at the 50 mg/kg dose. However, with a 100 mg/kg dose, no statistical difference was observed between nanoATV/r and FA-nanoATV/r. A possible explanation for this finding is that the spleen drug levels were sufficiently high in both 100 mg/kg dose groups (Figure S2) to lead to significant reduction in HIV-1*gag* RNA. In the chronic infected mice, viral RNA levels (RNA copies/ml) were monitored, before and after treatment. The average number of viral RNA copies/ml for treated (100 mg/kg FA-P407-ATV/r) and untreated (infected control) animals before treatment were 2.7×10^5 and 2.9×10^5 respectively. Following treatment, the FA-P407-ATV/r group contained two mice with undetectable viral levels, one with a 2-log decrease and another with a log decrease in viral RNA copies/ml compared to the untreated group. The untreated group had an average of 2.2×10^5 RNA viral copies/ml.

Discussion

Long-acting injectable nanoART is rapidly emerging as part of the general therapeutic armament for HIV/AIDS [2, 11, 31]. Active research resides in the discovery of new

hydrophobic drugs with longer half-lives and protein-binding capacities over what is more commonly prescribed [32, 33]. A key component of this research effort centers upon taking the drug formulations one step further than by simply improving drug half-life or maintaining therapeutic plasma drug concentrations. This can be achieved by facilitating drug levels in the cell and tissue depots and as well as targeting reservoir sites of persistent infection. One means to attain this goal is by placing specific targeting ligands on the surface of the nanoART formulation. This has now been achieved with FA. Here we report substantially improved PK and PD, with similar antiretroviral endpoints, for FA-nanoATV/r using a lower drug dose of 50 mg/kg, given as a parenteral injection, than what we have previously shown with 250 mg/kg P188-ATV/r. Notably, the latter were prepared without the FA coating [25]. We posit that such dosage forms can be administered once every 2 weeks or more infrequently [13]. Future studies will be made to validate this idea.

The advantages of targeted nanotherapies include the maintenance of therapeutic drug levels for weeks or months following a single parenteral administration, improved compliance and patient interest, sustained reductions in viral load, decreased viral resistance against ART regimens and, as shown in the current report, targeting of viral reservoirs [31, 34, 35]. As per the latter, we targeted folate receptors on macrophages by coating crystalline ARTs with FA-conjugated P407. This platform not only sustained plasma drug levels but also provided improved biodistribution to sites of viral reservoirs.

The FR is currently being used as a targeted nanoformulation drug scheme for a broad range of cancers, degenerative and inflammatory diseases. This approach serves as a novel means to improve disease diagnosis and treatment primarily for cancer and chronic inflammatory disorders [36–39]. Notably for ART nanoformulation development, expression of the FR is upregulated on activated macrophages. Such activation can occur from the interactions between nanoART and macrophages as has been previously described by our group [40]. We posit that FR overexpression on macrophages is clinically important for the progression of HIV-1 infection as sites of viral replication strongly coordinate with innate immune responses. Thus, using FA-P407-coated nanoART has both biological and pharmacological advantages. Disease sites including reservoirs for persistent viral infection can be readily targeted while sustained antiretroviral responses can be realized by engagement of the nanoART itself on the macrophage cell surface. Moreover, sites of disease, where physiological symptoms are notable, are coordinate with macrophage activation in the brain, lungs, lymphatics and GALT [41–43]. This coupled with observed advantages for intracellular endosomal storage [16] has led to the improved outcomes seen in PK and PD, as described in our current human cell reconstituted mouse studies. Moreover, such improvements extend our prior works demonstrating that cell-mediated drug delivery using nanoART yields appreciable improvement in PK and biodistribution of ART [12].

The dosage scheme developed herein has potential clinical application and could further reduce HIV/AIDS to an ever more manageable disease. Herein, we demonstrated the ability of these nanoformulations to reduce levels of infection in a HIV-1 murine model. To this end, HIV-1_{ADA} infected NSG mice reconstituted with hu-PBL and treated with FA-P407-ATV/r showed significantly improved antiretroviral responses over either native drug or non-targeted formulations. Interestingly, our FA-P407-coated formulations had similar

physicochemical characteristics to the parent P407-coated formulations. Both were ultrastructurally long rods with a negative surface charge. The formulations were stable at room temperature and hence are easily stored after lyophilization. However, significant differences between the formulations were observed in regards to cell entry related to receptor-mediated delivery of FA-nanoATV/r [13]. This finding was coordinate with FRβ expression on tissue macrophages. Moreover, the findings support the idea that macrophages can be a carrier of nanoART to divergent tissues [18, 19]. The co-localization of nanoART in macrophage endosomes further demonstrates a significant drug content in macrophage depots [16, 44].

Balb/cJ mice were administered FA-nanoATV/r and nanoATV/r, and plasma and tissue concentrations were determined. FA-P407-coated nanoART demonstrated up to a five times higher bioavailability at 14 days than non-targeted nanoART. Plasma drug levels were biphasic, suggesting two depots, the site of injection and another tissue (i.e., liver). FA-nanoATV/r demonstrated better penetration into lymph nodes and spleen than nanoATV/r. Even though similar pharmacokinetics were obtained in hu-PBL reconstituted mice, a high variation in plasma and tissue drug levels was observed. This could be due to the variability in the hu-PBL reconstitution. We investigated the immune parameters after treatment with three different doses of FA-nanoATV/r and compared the response to that of the nanoATV/r and PBS groups. To this end, CD4+ and CD8+ T cell populations were determined during and after treatment. Mice that were PBS-treated had a significant loss in CD4+ T cells compared to FA-nanoATV/r in spleen at all doses. Free drug treatment was also unable to prevent the depletion in CD4+ T cell counts at 10 mg/kg. At a free drug dose of 50 mg/kg, the drug appeared to precipitate out of solution and larger size particles were observed in the injection solution, causing severe immune reactions at the site of injection. Hence, free drug was not administered at a dose of 100 mg/kg. In contrast, FA-nanoATV/r protected against CD4+ T cell depletion; however, no statistical difference between FA-P407-coated and non-targeted nanoATV/r was observed but both treatments restored the CD4:CD8 ratios. One explanation for the lack of difference could be that CD4+ T cells require longer than 2 weeks for recovery in the hu-PBL mouse model and both treatments are equally effective at day 14. A greater difference in CD4+ T cell counts in response to FA-P407-ATV/r and P407-ATV/r treatment may be observed in a chronic HIV-1 humanized mouse model. Further investigation is necessary using CD34+ hematopoietic stem cell humanized mice. Additionally, it is interesting to note that statistical significance for differences in CD4:CD8+ T cell ratios between PBS treated and nanoformulation treated groups was achieved in the spleen, which is a viral reservoir, and not in the blood. This could be because of higher numbers of T cells in the spleen compared to blood.

In addition the spleen, liver and lungs of nanoART treated hu-PBL-NSG mice were probed with antibodies against HIV-1p24 and HLA-DR. At a dose of 50 mg/kg, 2/5 livers and 4/5 spleens had ≤ 2% HIVp24+ cells following FA-nanoATV/r treatment compared to 0/6 livers and 1/6 spleen following nanoATV/r treatment (Figure 5B). Percent of HIV-1p24+ cells among HLA-DR+ cells paralleled tissue drug levels. It is interesting to note that HIVp24+ cell quantitation was a better representation of the protection offered by FA-nanoATV/r than CD4+/CD8+ T cell ratios in the hu-PBL-NSG mouse model. Also, the percent of HIV-1p24+ cells was dose-dependent for both FA-targeted and non-targeted nanoART

treatments. We also examined HIV-1 replication in the spleen by PCR analyses. We observed that at the 50 mg/kg dose, FA-nanoATV/r suppressed HIV-1 replication to a significantly greater extent compared to nanoATV/r (Figure 6B). However, no difference was found at a dose of 100 mg/kg. This likely reflects the fact that at higher doses both treatments are equally effective. The 50 mg/kg dose of FA-P407-ATV/r demonstrated greatest differences in reducing HIV-1 infection. To cross validate PrEP FA-P407-ATV/r studies, four week HIV-1 infected mice were treated with FA-P407-ATV/r. The CD34+ HSC mice permit long-term engraftment of human cells. Every other week injection of 100mg/kg FA-P407-ATV/r resulted in up to or exceeding 2-log decreases in viral load as measured in copies/ml when compared against replicate untreated mice. These data serve to validate the effectiveness of FA-P407-ATV/r. Moreover, the findings suggest that 100 mg/kg FA-P407-ATV/r can effectively suppress ongoing viral replication.

It should be noted that a 50 mg/kg dose was a significant improvement over a 250 mg/kg dose of our first-generation non-targeted formulations [25]. This mouse dose is equivalent to a human dose of approximately 4 mg/kg based on the interspecies conversion scale of body surface area as recommended by the FDA [45]. Such a dose would solve two major problems with the present long-acting antiretroviral injectables. First, the volume of injection can be significantly reduced which makes an IM injection feasible in humans. Second, the therapeutic dose can be greatly reduced while achieving similar PK and PD outcomes.

Conclusions

We now demonstrate that FA-nanoATV/r significantly improves drug bioavailability, biodistribution and PD endpoints in HIV-1 infected mouse model. A major finding is the penetration of FA-nanoATV/r to lymphoid organs such as the spleen and lymph nodes. The PK and immune parameters are both dose-dependent. The CD4+/CD8+ T cell ratios were not statistically different between FA-targeted and non-targeted nanoATV/r groups; however, statistical significance was observed for reduction in percent of HIV-1p24+ cells and suppression of HIV-1*gag* RNA indicative of improved therapeutic effectiveness [46, 47]. A 50 mg/kg dose was the threshold for PD efficacy for FA-nanoATV/r. A biweekly administration of 100 mg/kg FA-nanoATV/r effectively reduced viral RNA levels up to 2 log times in an ongoing infection mouse model. In consideration of the advantages elicited by FA-nanoATV/r, it appears that this nanoformulation could be further considered for advancement to human testing.

Supplementary Material

Refer to Web version on PubMed Central for supplementary material.

Acknowledgments

This work was supported by the University of Nebraska Foundation that includes individual donations from Dr. Carol Swarts and Frances and Louie Blumkin; the Vice Chancellor for Research office, UNMC; ViiV Healthcare; and National Institutes of Health grants P01 MH64570, R01 MH104147, P01 DA028555, R01 NS36126, P01 NS31492, 2R01 NS034239, P01 NS43985, P30 MH062261, R01 AG043540 (H.E.G.) and the Intramural Research Program of the NIH, National Cancer Institute, Center for Cancer Research (D.S.D).

References

1. Ford SL, Gould E, Chen S, Margolis D, Spreen W, Crauwels H, et al. Lack of pharmacokinetic interaction between rilpivirine and integrase inhibitors dolutegravir and GSK1265744. Antimicrob Agents Chemother. 2013; 57:5472–7. [PubMed: 23979733]
2. Dolgin E. Long-acting HIV drugs advanced to overcome adherence challenge. Nature medicine. 2014; 20:323–4.
3. Bangsberg DR, Hecht FM, Charlebois ED, Zolopa AR, Holodniy M, Sheiner L, et al. Adherence to protease inhibitors, HIV-1 viral load, and development of drug resistance in an indigent population. Aids. 2000; 14:357–66. [PubMed: 10770537]
4. Fogarty L, Roter D, Larson S, Burke J, Gillespie J, Levy R. Patient adherence to HIV medication regimens: a review of published and abstract reports. Patient education and counseling. 2002; 46:93–108. [PubMed: 11867239]
5. Puigventos F, Riera M, Delibes C, Penaranda M, de la Fuente L, Boronat A. Adherence to antiretroviral drug therapy. A systematic review. Medicina clinica. 2002; 119:130–7. [PubMed: 12106524]
6. Bartlett JA, Shao JF. Successes, challenges, and limitations of current antiretroviral therapy in low-income and middle-income countries. The Lancet infectious diseases. 2009; 9:637–49. [PubMed: 19778766]
7. Baum MK, Rafie C, Lai S, Sales S, Page B, Campa A. Crack-cocaine use accelerates HIV disease progression in a cohort of HIV-positive drug users. J Acquir Immune Defic Syndr. 2009; 50:93–9. [PubMed: 19295339]
8. Towards Universal access. Progress report. 2008. Scaling up priority HIV/AIDS interventions in the health sector.
9. Antoniou T, Tseng AL. Interactions between recreational drugs and antiretroviral agents. The Annals of pharmacotherapy. 2002; 36:1598–613. [PubMed: 12243611]
10. Rabinow BE. Nanosuspensions in drug delivery. Nat Rev Drug Discov. 2004; 3:785–96. [PubMed: 15340388]
11. Spreen WR, Margolis DA, Pottage JC Jr. Long-acting injectable antiretrovirals for HIV treatment and prevention. Curr Opin HIV AIDS. 2013; 8:565–71. [PubMed: 24100877]
12. Gautam N, Roy U, Balkundi S, Puligujja P, Guo D, Smith N, et al. Preclinical pharmacokinetics and tissue distribution of long-acting nanoformulated antiretroviral therapy. Antimicrobial agents and chemotherapy. 2013; 57:3110–20. [PubMed: 23612193]
13. Puligujja P, McMillan J, Kendrick L, Li T, Balkundi S, Smith N, et al. Macrophage folate receptor-targeted antiretroviral therapy facilitates drug entry, retention, antiretroviral activities and biodistribution for reduction of human immunodeficiency virus infections. Nanomedicine: Nanotechnology, Biology and Medicine. 2013; 9:1263–73.
14. Alexaki A, Liu Y, Wigdahl B. Cellular reservoirs of HIV-1 and their role in viral persistence. Current HIV research. 2008; 6:388–400. [PubMed: 18855649]
15. Rao KS, Ghorpade A, Labhasetwar V. Targeting anti-HIV drugs to the CNS. Expert opinion on drug delivery. 2009; 6:771–84. [PubMed: 19566446]
16. Guo D, Zhang G, Wysocki TA, Wysocki BJ, Gelbard HA, Liu XM, et al. Endosomal Trafficking of Nanoformulated Antiretroviral Therapy Facilitates Drug Particle Carriage and HIV Clearance. Journal of virology. 2014 In Press.
17. van't Klooster G, Hoeben E, Borghys H, Looszova A, Bouche MP, van Velsen F, et al. Pharmacokinetics and disposition of rilpivirine (TMC278) nanosuspension as a long-acting injectable antiretroviral formulation. Antimicrob Agents Chemother. 2010; 54:2042–50. [PubMed: 20160045]
18. Nowacek AS, Miller RL, McMillan J, Kanmogne G, Kanmogne M, Mosley RL, et al. NanoART synthesis, characterization, uptake, release and toxicology for human monocyte-macrophage drug delivery. Nanomedicine (Lond). 2009; 4:903–17. [PubMed: 19958227]
19. Balkundi S, Nowacek AS, Roy U, Martinez-Skinner A, McMillan J, Gendelman HE. Methods development for blood borne macrophage carriage of nanoformulated antiretroviral drugs. Journal of visualized experiments: JoVE. 2010

20. Clark SC. Interleukin-6. Multiple activities in regulation of the hematopoietic and immune systems. Ann N Y Acad Sci. 1989; 557:438–43. [PubMed: 2660700]
21. Dou H, Destache CJ, Morehead JR, Mosley RL, Boska MD, Kingsley J, et al. Development of a macrophage-based nanoparticle platform for antiretroviral drug delivery. Blood. 2006; 108:2827–35. [PubMed: 16809617]
22. Poluektova LY, Munn DH, Persidsky Y, Gendelman HE. Generation of cytotoxic T cells against virus-infected human brain macrophages in a murine model of HIV-1 encephalitis. Journal of immunology. 2002; 168:3941–9.
23. Huang J, Gautam N, Bathena SP, Roy U, McMillan J, Gendelman HE, et al. UPLC-MS/MS quantification of nanoformulated ritonavir, indinavir, atazanavir, and efavirenz in mouse serum and tissues. Journal of chromatography B, Analytical technologies in the biomedical and life sciences. 2011; 879:2332–8.
24. Gorantla S, Makarov E, Finke-Dwyer J, Gebhart CL, Domm W, Dewhurst S, et al. CD8+ cell depletion accelerates HIV-1 immunopathology in humanized mice. Journal of immunology. 2010; 184:7082–91.
25. Roy U, McMillan J, Alnouti Y, Gautum N, Smith N, Balkundi S, et al. Pharmacodynamic and antiretroviral activities of combination nanoformulated antiretrovirals in HIV-1-infected human peripheral blood lymphocyte-reconstituted mice. The Journal of infectious diseases. 2012; 206:1577–88. [PubMed: 22811299]
26. Dash PK, Gorantla S, Gendelman HE, Knibbe J, Casale GP, Makarov E, et al. Loss of neuronal integrity during progressive HIV-1 infection of humanized mice. The Journal of neuroscience: the official journal of the Society for Neuroscience. 2011; 31:3148–57. [PubMed: 21368026]
27. Nowacek AS, McMillan J, Miller R, Anderson A, Rabinow B, Gendelman HE. Nanoformulated antiretroviral drug combinations extend drug release and antiretroviral responses in HIV-1-infected macrophages: implications for neuroAIDS therapeutics. Journal of neuroimmune pharmacology: the official journal of the Society on NeuroImmune Pharmacology. 2010; 5:592–601. [PubMed: 20237859]
28. Nowacek AS, Balkundi S, McMillan J, Roy U, Martinez-Skinner A, Mosley RL, et al. Analyses of nanoformulated antiretroviral drug charge, size, shape and content for uptake, drug release and antiviral activities in human monocyte-derived macrophages. J Control Release. 2011; 150:204–11. [PubMed: 21108978]
29. HHS Panel on Antiretroviral Guidelines for Adults and Adolescents OoARACO. Guidelines for the Use of Antiretroviral Agents in HIV-1-Infected Adults and Adolescents. 2014. http://aidsinfo.nih.gov/ContentFiles/AdultandAdolescentGL.pdf
30. Dash PK, Gendelman HE, Roy U, Balkundi S, Alnouti Y, Mosley RL, et al. Long-acting nanoformulated antiretroviral therapy elicits potent antiretroviral and neuroprotective responses in HIV-1-infected humanized mice. Aids. 2012; 26:2135–44. [PubMed: 22824628]
31. Williams J, Sayles HR, Meza JL, Sayre P, Sandkovsky U, Gendelman HE, et al. Long-acting parenteral nanoformulated antiretroviral therapy: interest and attitudes of HIV-infected patients. Nanomedicine (Lond). 2013; 8:1807–13. [PubMed: 23611617]
32. Taha H, Morgan J, Das A, Das S. Parenteral patent drug S/GSK1265744 has the potential to be an effective agent in pre-exposure prophylaxis against HIV infection. Recent patents on anti-infective drug discovery. 2013; 8:213–8. [PubMed: 24738551]
33. Balkundi S, Nowacek AS, Veerubhotla RS, Chen H, Martinez-Skinner A, Roy U, et al. Comparative manufacture and cell-based delivery of antiretroviral nanoformulations. International journal of nanomedicine. 2011; 6:3393–404. [PubMed: 22267924]
34. Nel A, Swindells S, Bronich T, Gendelman HE. Interview: Nanomedicine and the fight against HIV/AIDS. Nanomedicine (Lond). 2014; 9:193–206. [PubMed: 24552561]
35. Mallipeddi R, Rohan LC. Progress in antiretroviral drug delivery using nanotechnology. International journal of nanomedicine. 2010; 5:533–47. [PubMed: 20957115]
36. Kularatne SA, Low PS. Targeting of nanoparticles: folate receptor. Methods in molecular biology. 2010; 624:249–65. [PubMed: 20217601]
37. Nukolova NV, Oberoi HS, Cohen SM, Kabanov AV, Bronich TK. Folate-decorated nanogels for targeted therapy of ovarian cancer. Biomaterials. 2011; 32:5417–26. [PubMed: 21536326]

38. Song S, Tian B, Chen F, Zhang W, Pan Y, Zhang Q, et al. Potentials of proniosomes for improving the oral bioavailability of poorly water-soluble drugs. Drug development and industrial pharmacy. 2013
39. Muller A, Beck K, Rancic Z, Muller C, Fischer CR, Betzel T, et al. Imaging atherosclerotic plaque inflammation via folate receptor targeting using a novel 18F-folate radiotracer. Molecular imaging. 2014; 13:1–11. [PubMed: 24622812]
40. Martinez-Skinner AL, Veerubhotla RS, Liu H, Xiong H, Yu F, McMillan JM, et al. Functional proteome of macrophage carried nanoformulated antiretroviral therapy demonstrates enhanced particle carrying capacity. Journal of proteome research. 2013; 12:2282–94. [PubMed: 23544708]
41. Crowe S, Zhu T, Muller WA. The contribution of monocyte infection and trafficking to viral persistence, and maintenance of the viral reservoir in HIV infection. Journal of leukocyte biology. 2003; 74:635–41. [PubMed: 12960232]
42. Dandekar S. Pathogenesis of HIV in the gastrointestinal tract. Current HIV/AIDS reports. 2007; 4:10–5. [PubMed: 17338855]
43. Bergamaschi A, Pancino G. Host hindrance to HIV-1 replication in monocytes and macrophages. Retrovirology. 2010; 7:31. [PubMed: 20374633]
44. Kadiu I, Nowacek A, McMillan J, Gendelman HE. Macrophage endocytic trafficking of antiretroviral nanoparticles. Nanomedicine (Lond). 2011; 6:975–94. [PubMed: 21417829]
45. M3(R2) Nonclinical Safety Studies for the Conduct of Human Clinical Trials and Marketing Authorization for Pharmaceuticals. 2010.
46. Poluektova L, Gorantla S, Faraci J, Birusingh K, Dou H, Gendelman HE. Neuroregulatory events follow adaptive immune-mediated elimination of HIV-1-infected macrophages: studies in a murine model of viral encephalitis. Journal of immunology. 2004; 172:7610–7.
47. Berges BK, Rowan MR. The utility of the new generation of humanized mice to study HIV-1 infection: transmission, prevention, pathogenesis, and treatment. Retrovirology. 2011; 8:65. [PubMed: 21835012]

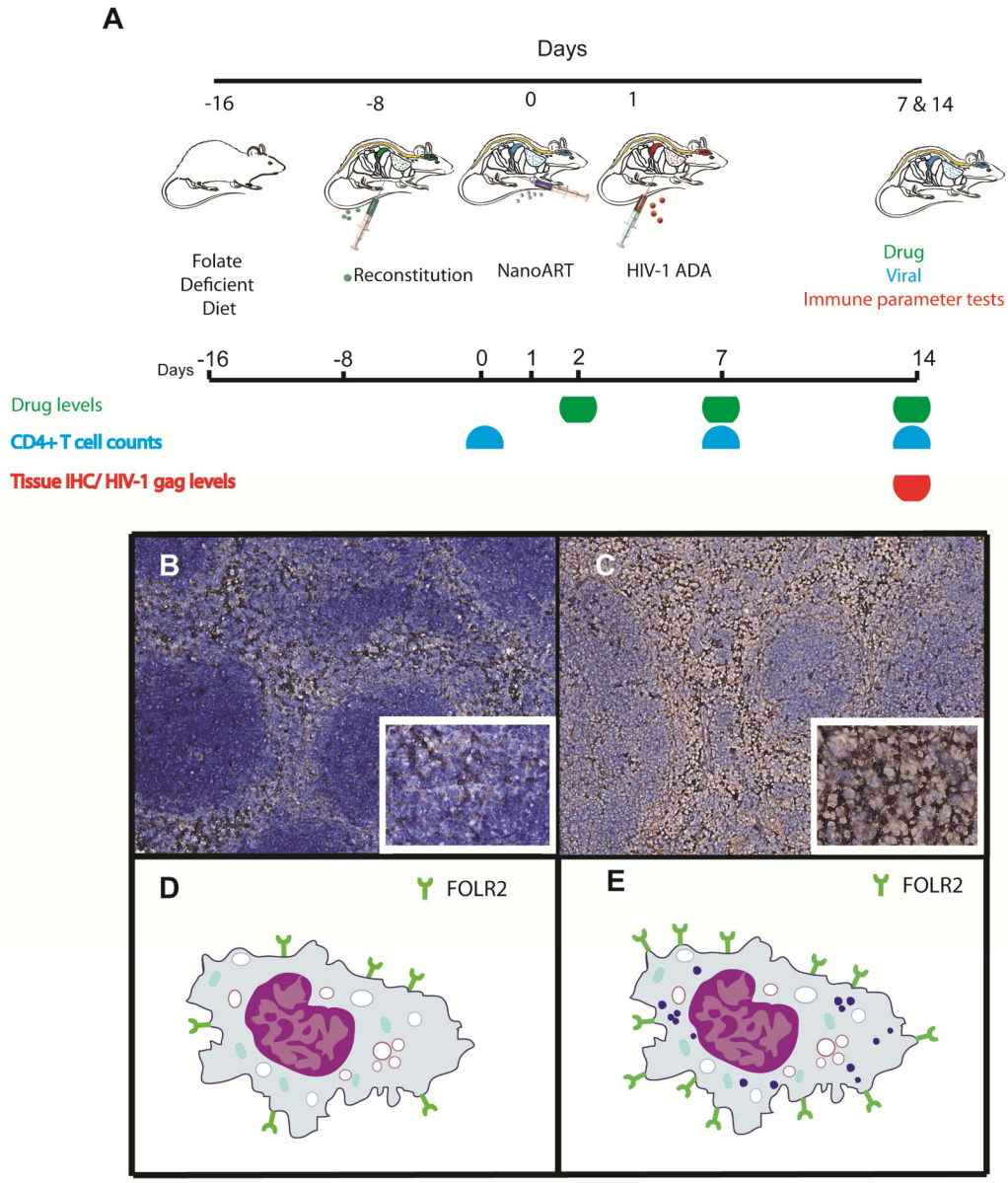

Figure 1.

(A) Treatment paradigm to determine pharmacokinetics, biodistribution, efficacy and toxicology profiles of nanoformulated antiretrovirals in human-peripheral blood lymphocyte reconstituted non-obese diabetic, severe combined immunodeficient mice (Hu-PBL-NSG mice); Cartoon schematic showing the advantage of targeting folate receptor-β on macrophage. A representative photomicrograph shows the expression of mouse folate receptor β (mFRβ) in spleen 36 hrs after treatment with (B) PBS and (C) nanoART. Balb/cJ mice were injected intramuscularly with PBS or nanoATV/r (100 mg/kg). Mice were sacrificed 36 hrs after treatment, and spleen sections were probed with a mFRβ-specific antibody using the Vertex M.O.M kit. Nuclei were stained with hematoxylin. The cartoon represents expression of FRβ on macrophages in spleen following (D) PBS and (E) nanoART treatment.

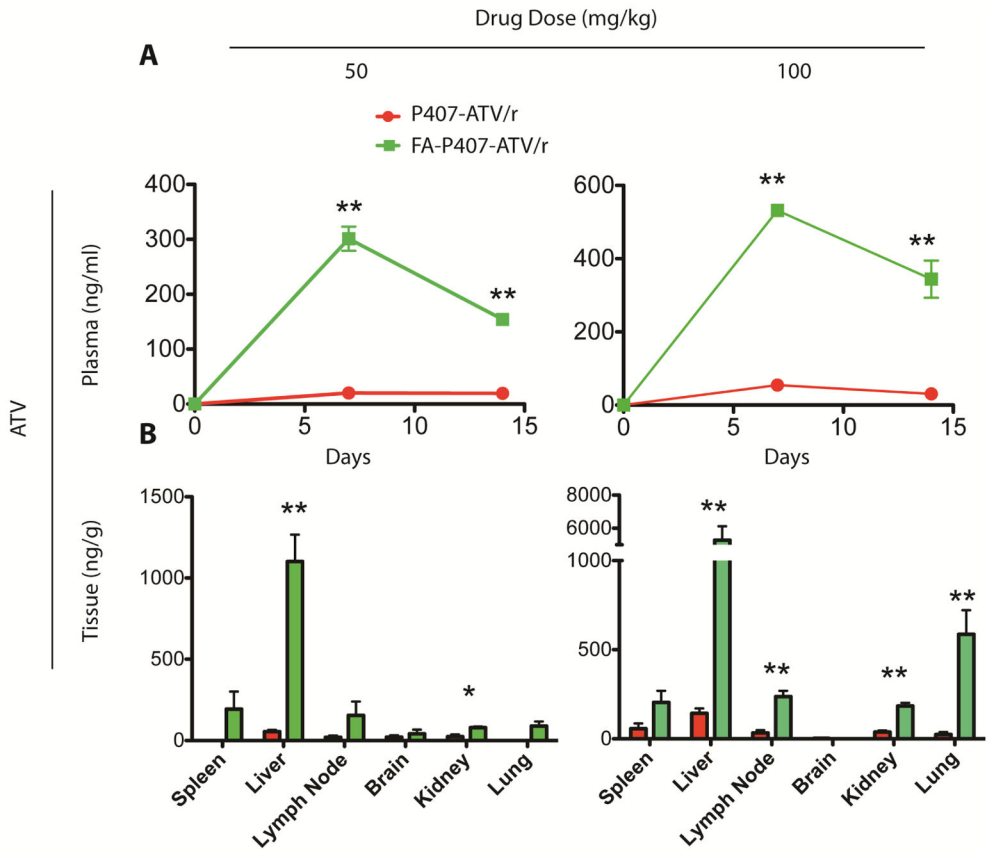

Figure 2.

Pharmacokinetics of FA-P407- and P407- ATV/r in Balb/cJ mice. FA-P407-ATV/r and P407-ATV/r were administered at a dose of 50 mg/kg or 100 mg/kg by intramuscular injection on day 0, and mice were sacrificed on day 14. **(A)** Plasma was collected at indicated time points and ATV and RTV levels were quantified by UPLC-MS/MS. Data are expressed as mean ± SEM. * Statistically different from P407-ATV/r at $P < 0.05$ by 2-way ANOVA and Bonferroni's posthoc test. **(B)** Comparison of tissue distribution of ATV and RTV after FA-P407-ATV/r and P407-ATV/r treatment in Balb/cJ mice. The indicated tissues were collected on day 14 after sacrifice, and ATV and RTV levels were quantified by UPLC-MS/MS. Data are expressed as mean ± SEM and *, **statistically different from P407-ATV/r at $P < 0.05$ and $P < 0.01$ by student's unpaired t-test respectively.

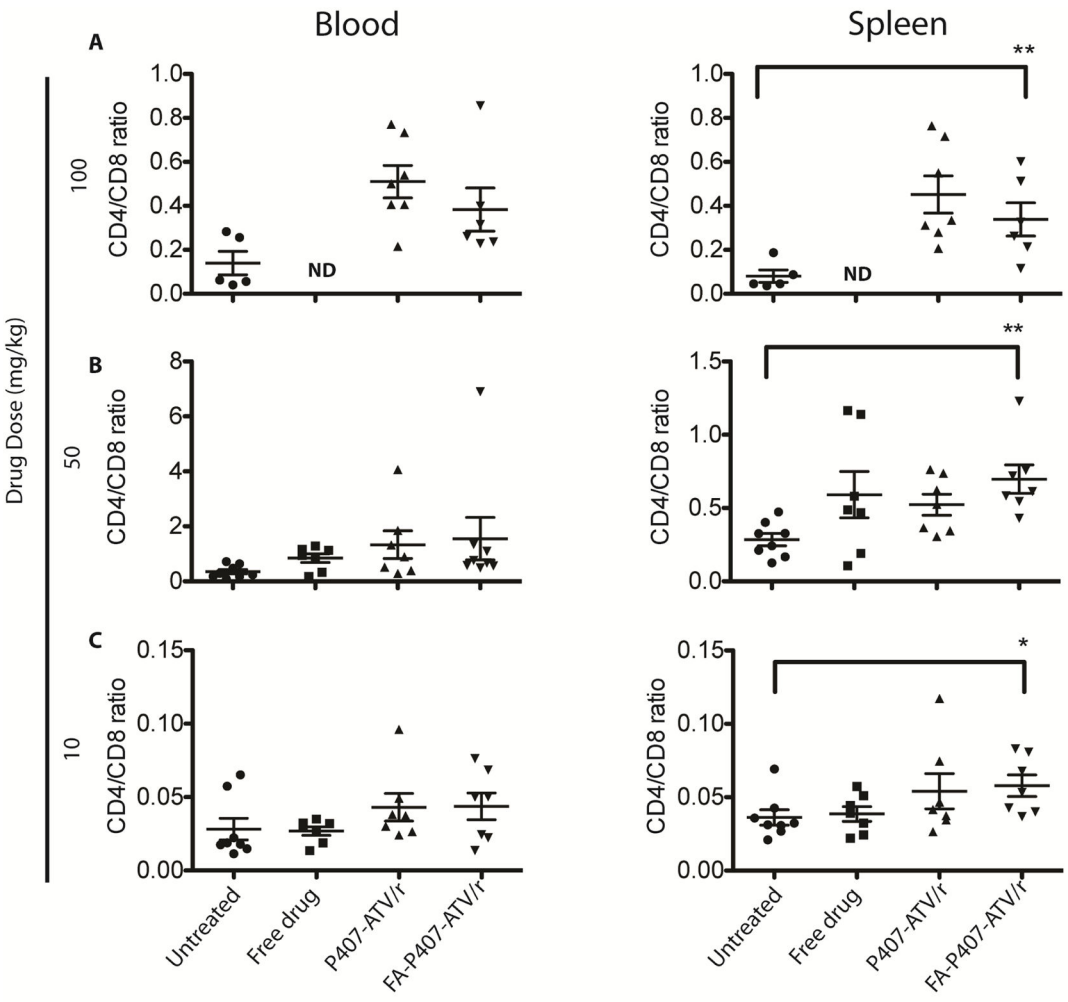

Figure 3.

Flow cytometric evaluation of FA-P407-ATV/r and P407-ATV/r in hu-PBL reconstituted NSG mice infected with HIV-1_{ADA}. On day 0, PBS, Free drug or nanoATV/r (a combination of ATV and rRTV) was delivered to PBL–reconstituted NSG mice at doses (A) 100 mg/kg, (B) 50 mg/kg or (C) 10 mg/kg. Mice were then infected with HIV-1_{ADA} on day 1 and sacrificed on day 14. Fluorescence-activated cell sorting analyses show the ratio of human CD4+ to CD8+ T cells among total CD3+ T cells for peripheral blood and spleen from individual mice. Data are means ± SEM and *, **statistically different at $P < 0.05$ and $P < 0.01$ by Mann-Whitney U-test.

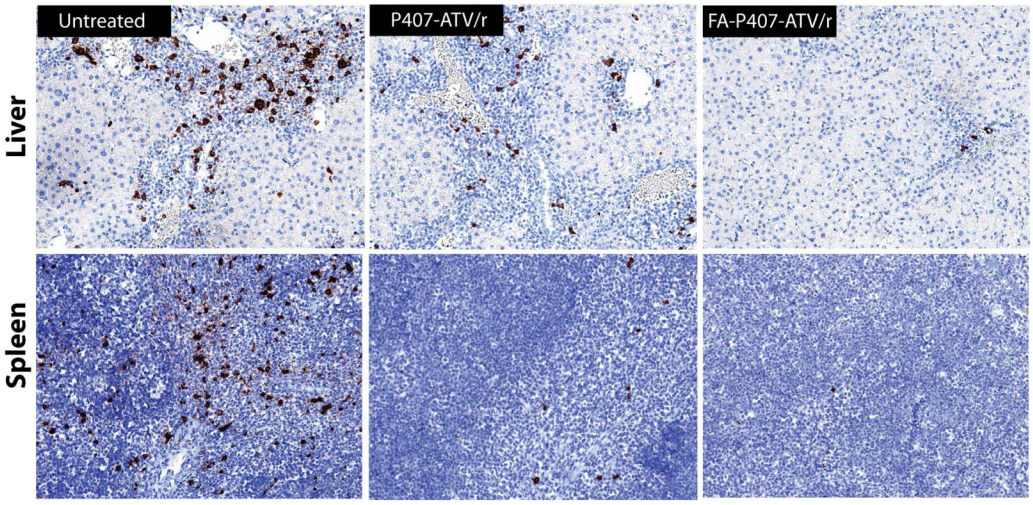

Figure 4.

Levels of HIV-1p24 antigen in liver and spleen of HIV-1 infected huPBL-reconstituted NSG mice treated with FA-P407-ATV/r and P407-ATV/r. FA-P407-ATV/r and P407-ATV/r (100 mg/kg each drug) were administered intramuscularly on day 0 to huPBL- NSG mice. Mice were infected with HIV-1_{ADA} on day 1 and sacrificed on day 14. Livers and spleens were collected on day 14 after drug injection, then sectioned and immunostained with antibodies specific for HLA-DR or HIV-1p24, and visualized by DAB.

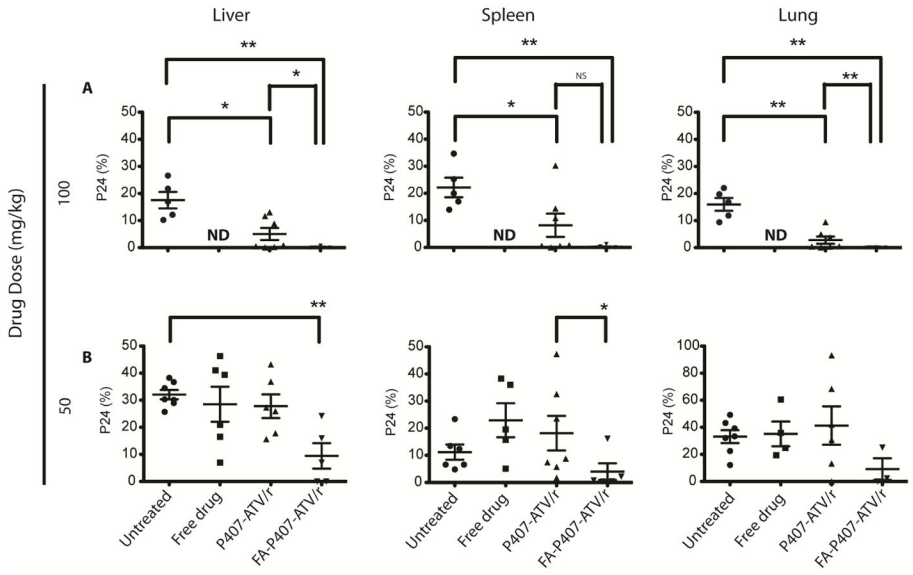

Figure 5.

Comparison of antiretroviral activities of FA-P407-ATV/r and P407-ATV/r in hu-PBL reconstituted NSG mice infected with HIV-1_{ADA}. Mice were treated on day 0 with PBS, free drug ATV/r, P407-ATV/r or FA-P407-ATV/r at doses of (**A**) 100 mg/kg or (**B**) 50 mg/kg. Mice were then infected with HIV-1_{ADA} on 24 hours later and sacrificed on day 14. Paraffin embedded sections of liver, spleen and lung were probed for HIV-1p24 and HLA-DR. Antiretroviral efficacy was determined by counting the number of HIV-1p24+ cells per section and expressed as percent of HLA-DR+ cells. Data are expressed as mean ± SEM and *, **statistical differences were determined at $P < 0.05$ and $P < 0.01$ by the Mann-Whitney U-test.

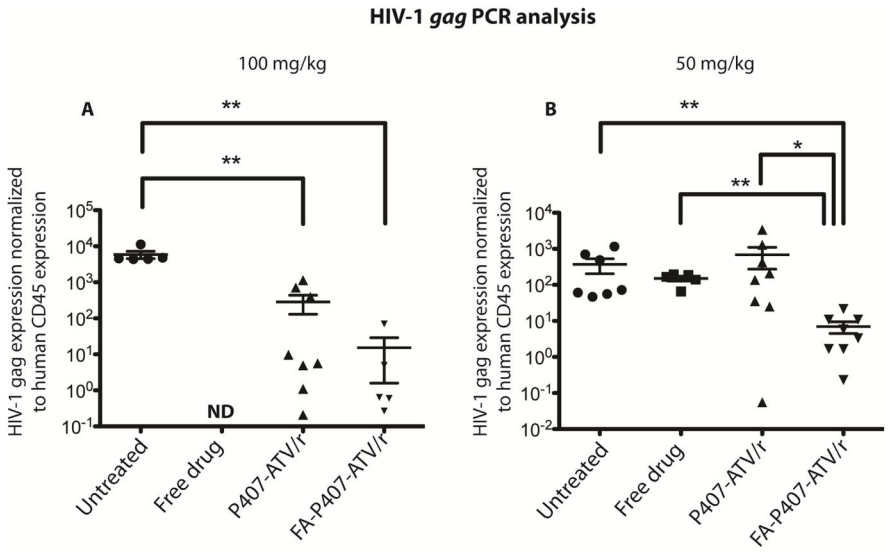

Figure 6.

Comparison of antiretroviral activities of FA-P407-ATV/r and P407-ATV/r in hu-PBL reconstituted NSG mice infected with HIV-1_{ADA}. Mice were treated on day 0 with PBS (untreated), free drug ATV/r, P407-ATV/r or FA-P407-ATV/r at doses of (**A**) 100 mg/kg or (**B**) 50 mg/kg. Mice were then infected with HIV-1_{ADA} 24 hours later and sacrificed on day 14. HIV-1*gag* RNA expression in spleen was determined and normalized to human CD45 expression as a marker for human cell reconstitution. Data are expressed as mean ± SEM and considered *, ** statistically different, at $P < 0.05$ and $P < 0.01$, by the Mann-Whitney U-test.